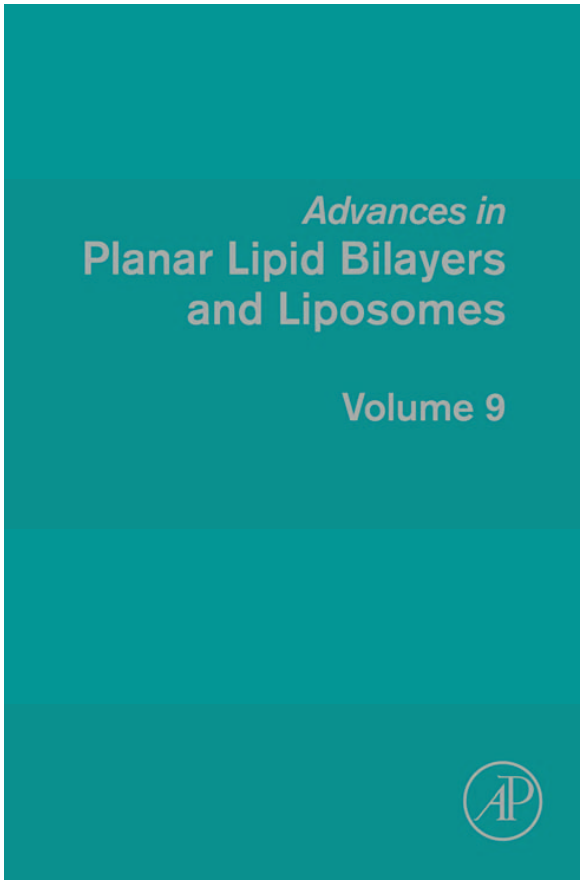

From: Klemen Bohinc, Jasna Zelko, P.B. Sunil Kumar, Aleš Iglič, and Veronika Kralj-Iglič, Attraction of Like-Charged Surfaces Mediated by Spheroidal Nanoparticles with Spatially Distributed Electric Charge: Theory and Simulation. In A. Leitmannova Liu and H.T. Tien, editors: Advances in Planar Lipid Bilayers and Liposomes, Vol. 9, Burlington: Academic Press, 2009, pp. 279-301.
ISBN: 978-0-12-374822-5

CHAPTER TEN

Attraction of Like-Charged Surfaces Mediated by Spheroidal Nanoparticles with Spatially Distributed Electric Charge: Theory and Simulation

Klemen Bohinc,[1,2] Jasna Zelko,[3] P.B. Sunil Kumar,[4] Aleš Iglič,[2,*] *and* Veronika Kralj-Iglič[3]

Contents

Abstract

The interaction between equal, uniformly charged flat surfaces, separated by a solution of spheroidal nanoparticles was studied theoretically. The nanoparticles were assumed to have spatially distributed electric charge. The nonlocal Poisson–Boltzmann (PB) theory for the spheroidal nanoparticles, which play the role of counterions, was developed. In the model the center of the spheroidal nanoparticle could not approach the charged surfaces closer than the radius of the nanoparticle. It was shown that for large enough diameters of nanoparticles

* Corresponding author. Tel.: +386 31 356 953; Fax: +386 1 4768 850;
E-mail address: ales.iglic@fe.uni-lj.si

[1] Laboratory of Physics, Faculty of Electrical Engineering, University of Ljubljana, Slovenia
[2] Faculty of Health Studies, University of Ljubljana, Slovenia
[3] Laboratory of Clinical Biophysics, Faculty of Medicine, University of Ljubljana, Slovenia
[4] Department of Physics, Indian Institute of Technology Madras, Chennai, India

Advances in Planar Lipid Bilayers and Liposomes, Volume 9
ISSN 1554-4516, DOI: 10.1016/S1554-4516(09)09010-3

and large enough surface charge densities of membrane surfaces, the two equally charged surfaces could experience an attractive force due to the spatially distributed charges within the nanoparticles. The results presented in this chapter may add to a better understanding of the coalescence of negatively charged membrane surfaces induced by positively charged nanoparticles (e.g., proteins) which are proposed to play an important role in the complex vital processes such as blood clot formation.

1. Introduction

The outer surface of biological membranes is usually negatively charged [1]. For example, blood involves negatively charged red blood cells [2, 3]. Also the outer membrane surface of the membrane microvesicles released from red blood cells, platelets, and lymphocytes, as well as from apoptotic cells (with negatively charged cardiolipin and phosphatidylserine in the outer membrane layer) are negatively charged [4–8].

Clinical evidence indicates that microvesicles are prothrombogenic, as they form catalytic surfaces for reactions of blood clot formation. A mechanism which could be relevant in microvesiculation is the coalescence of negatively charged membraneous structures mediated by multivalent ions [9–11]. Possible candidates for such multivalent polyions could be various membrane proteins, including antibodies [9–12] and also artificial nanoparticles (entering the body from the environment). Spheroidal multivalent ions (nanoparticles) may thus play an important role in the formation of blood clots.

The phenomena of ion-mediated attractive interaction between two equally charged surfaces has been observed previously in many other cases as well. The first experimental observation of attraction between two highly negatively charged clays was reported for $CaCl_2$ solution [13, 14]. Attraction between charged lamellae [15], DNA condensation [16–18], network formation in actin solutions [19], complexation of DNA with positively charged colloidal particles [20], and virus aggregation [21] have also been observed. However, origins of these attractive interactions are still not fully understood.

Theory of equally charged surfaces separated by a solution containing dimensionless ions in the mean field approach yields electrostatic repulsion [22–25]. However, it was indicated recently that large multivalent ions in solution between two equally charged surfaces can induce at close distances, also an attractive force between these two surfaces [26, 27]. Monte Carlo simulations showed the existence of attractive interaction between equally charged surfaces immersed in a solution composed of multivalent ions in the limit of high surface charge densities [28–31]. Therefore, different improvements with respect to Poisson–Boltzmann (PB) theory were suggested in order to explain the observed attraction between like-charged surfaces. Among others, direct ion–ion interactions were considered as a possible explanation for attractive interaction within hypernetted chain theory

[32–35], density functional theories [36–39], and by taking into account in-plane Gaussian fluctuations [40–42].

New fields of research interest that were opened in past decade offer new possibilities for the application of modified PB theories, especially in the study of polyelectrolyte solutions [43, 44] and of protein–membrane interactions [45–48]. In such systems, charge distribution along the polyelectrolyte chain or within the protein is essential to explain the attraction between two like-charged membranes. Bridging mechanism, where polyions are oriented in such a way that they electrostatically bind together the neighboring equally charged surfaces, was proposed in the case of polyelectrolyte-induced attraction between two charged surfaces [43, 44, 49]. Electrostatic interactions may also play a crucial role in interaction of proteins with the membrane. It was suggested that charge distribution within a protein influences the orientation of the protein at the membrane surface [50].

The importance of finite ion size [51–54] and charge distribution [55] in polyions for their solvation and double layer effects has been considered previously. If spheroidal multivalent nanoparticles have an internal charge distribution with charges being located at different, well-separated positions [56], the classical PB description of the electric double layer fails to describe the experimentally obtained spatial distribution and orientation of the multivalent nanoparticles [57]. A generalization of the PB theory of the electric double layer for the case of multivalent nanoparticles could be made by taking into account the internal space charge distribution of a single spheroidal multivalent nanoparticle [58]. Theoretical description of such large multivalent spheroidal nanoparticles in between two planar charged surfaces that takes into account the internal charge distribution was proposed recently [56], using a simple three-state model for the orientation of the multivalent ions in the gradient of the electric field and applying the methods of statistical physics. It was assumed that the distance between the electric charges within a single multivalent nanoparticle is small enough to justify the Taylor series expansion [58] in calculation of the electrostatic energy of a single spheroidal multivalent nanoparticle in the electric field gradient [56]. The orientational ordering of the multivalent nanoparticles near the charged membrane surface was predicted [56]. However, within this model the internal space charge distribution was taken into account only in the entropic part of the free energy.

In this work we present a theoretical model with an improved description of the effect of the spatial charge distribution within the spheroidal nanoparticle on the electric field and the free energy of the system. In our case the two charges are placed oppositely on a surface of the spherical nanoparticle; however, the theory presented can be generalized to include any separation between charges within the spherical nanoparticle. The distance of closest approach of the spherical nanoparticles to the charged surface was taken into account [59] while the direct particle–particle hard core interactions were not taken into account.

2. Theoretical Model

We consider an aqueous solution containing spheroidal (Fig. 1) multivalent nanoparticles, which are positively charged and have a diameter a. In the model the electric charge of each spheroidal nanoparticle is described by two equal charges $e = Ze_0$, separated by an arbitrary distance l, where Z is the valency and e_0 the elementary charge. The solution is sandwiched between two large, planar surfaces of area A (Fig. 2), each carrying a uniform negative surface charge density σ. The distance between the two surfaces is D. For the sake of simplicity we take $l = a$. The volume of the spheroidal nanoparticle is given by $v_0 = (4\pi/3)(a/2)^3$. The electrostatic field between the two charged surfaces varies only in the direction normal to the surfaces (x-direction). We assume that there is no electric field on the other side of each charged plate.

For each spheroidal nanoparticle, the center of the charge distribution (also its geometric center) is located at x. The two point charges are located at geometrically opposite points separated by a distance l. When projected onto the x-axis, their positions are at $x + s$ and $x - s$ respectively, as shown in Fig. 2. We describe the spheroidal nanoparticles by the local concentration of nanoparticles $n(x)$. Furthermore, we refer to one of the charges of the nanoparticle as the reference charge. The location of the reference charge of a given spheroidal nanoparticle is specified by the conditional probability $p(s|x)$, x denoting the location of the center of the nanoparticle. The probability density $p(s|x)$ satisfies the relation

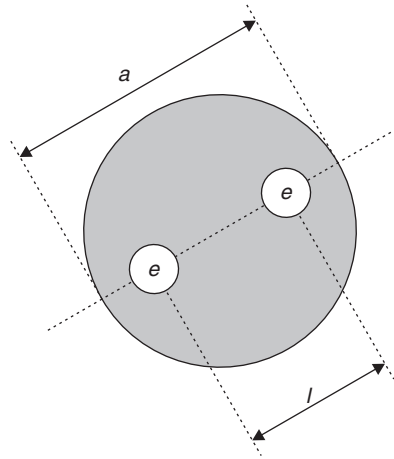

Figure 1 Schematic diagram of a large spheroidal multivalent nanoparticle with net electric charge $2e$ and average diameter a. In the model the space charge distribution of the multivalent nanoparticle is described by two effective polyions of charge e located at different, well-separated positions $l \leq a$. The main axis of the nanoparticle coincides with the line connecting the two polyions.

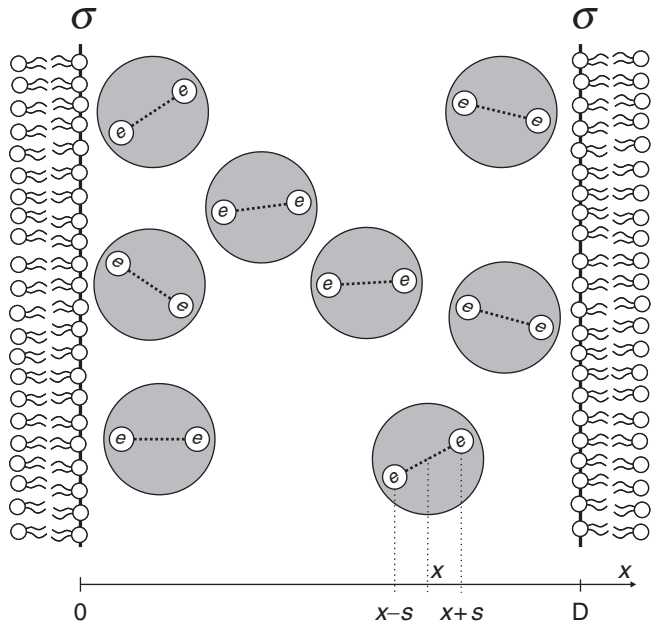

Figure 2 Schematic illustration of two like-charged planar cell surfaces of surface charge density σ, interacting in a solution that contains multivalent spheroidal nanoparticles. The coordinate x specifies the center of the spheroidal nanoparticle while the coordinates $x - s$ and $x + s$ specify the positions of two charges in a spheroidal nanoparticles. The distance between the planar surfaces is D.

$$\frac{1}{l}\int_{-l/2}^{l/2} p(s|x)\mathrm{d}s = 1 \tag{1}$$

and $p(s|x) = 0$ for any x and $|s| > l/2$.

The electrostatic free energy of the system F measured per unit area A and expressed in units of the thermal energy kT (here k is the Boltzmann constant and T is the absolute temperature) can be expressed as

$$\frac{F}{AkT} = \int_{-\infty}^{\infty} \mathrm{d}x \left[\frac{\Psi'(x)^2}{8\pi l_\mathrm{B}} + n(x)\ln n(x)\nu_0 + \frac{1}{\nu_0}(1 - n(x)\nu_0). \right.$$
$$\left. \ln(1 - n(x)\nu_0) + n(x)\langle p(s|x)[\ln p(s|x) + U(x)]\rangle \right] \tag{2}$$

where the first term is the electrostatic energy, the second and the third terms are contributions to the positional entropy including the excluded volume effect and the fourth term is the orientational entropy. The reduced

electrostatic potential is denoted by Ψ where $l_B = \frac{e_0^2}{4\pi\varepsilon\varepsilon_0 kT}$ is the Bjerrum length, ε is the dielectric constant of the solution and ε_0 is the permittivity of the vacuum. The average of an arbitrary function $g(s)$ is defined as

$$\langle g(s)\rangle = \frac{1}{l}\int_{-l/2}^{l/2} g(s)\mathrm{d}s \tag{3}$$

while the function

$$U(x) = \begin{cases} 0, & \frac{l}{2} \le x \le D - \frac{l}{2} \\ \infty, & \text{elsewhere} \end{cases} \tag{4}$$

is introduced in order to ensure that the spheroidal nanoparticles are confined within the region specified by the charged walls.

Equation (2) can be written in the following form:

$$\begin{aligned} \frac{F}{AkT} = \int_{-\infty}^{\infty} \mathrm{d}x \Bigg[& \frac{\Psi'(x)^2}{8\pi l_B} + n(x)\ln\, n(x)\nu_0 - n(x) \\ & + \gamma\left[\frac{1}{\nu_0}(1 - n(x)\nu_0)\ln(1 - n(x)\nu_0) + n(x)\right] \\ & + n(x)\langle p(s|x)[\ln\, p(s|x) + U(x)]\rangle\Bigg] \end{aligned} \tag{5}$$

where we introduce parameter γ as

$$\gamma = \begin{cases} 0, & \text{excluded volume not taken into acount} \\ 1, & \text{excluded volume taken into acount} \end{cases} \tag{6}$$

The equilibrium state of the system is determined by the minimum of the total free energy F, subject to the constraints that (1) the orientational probability of the spheroidal nanoparticles, integrated over all possible projections (Eq. (1)), is equal to 1 and that (2) the system is electroneutral $\left(2Z\int_{-\infty}^{\infty} n(x)\mathrm{d}x = 2\sigma/e_0\right)$. To solve this variational problem, a functional $\int_{-\infty}^{\infty}\mathcal{F}\mathrm{d}x$ is constructed:

$$\begin{aligned} \int_{-\infty}^{\infty}\mathcal{F}\mathrm{d}x = \frac{F}{AkT} + & \int_{-\infty}^{\infty}\lambda(x)n(x)\left(\frac{1}{l}\int_{-l/2}^{l/2} p(s|x)\mathrm{d}s - 1\right)\mathrm{d}x \\ & + \mu\int_{-\infty}^{\infty}\left[2Zn(x) - \frac{2\sigma}{e_0 D}\right]\mathrm{d}x \end{aligned} \tag{7}$$

where $\lambda(x)$ and μ are the local and global Lagrange multipliers, respectively. By taking into account Eq. (5), we can rewrite Eq. (7) in the form

$$\begin{aligned}\int_{-\infty}^{\infty}\mathcal{F}\,\mathrm{d}x = \int_{-\infty}^{\infty}\mathrm{d}x\Bigg[&\frac{\Psi'(x)^2}{8\pi l_B} + n(x)\ln(n(x)v_0)\\ &- n(x) + \gamma\left[\frac{1}{v_0}(1-n(x)v_0)\ln(1-n(x)v_0) + n(x)\right]\\ &+ n(x)\langle p(s|x)[\ln p(s|x) + U(x)]\rangle\Bigg]\\ &+ \int_{-\infty}^{\infty}\mathrm{d}x\; n(x)\lambda(x)[\langle p(s|x)\rangle - 1]\\ &+ \mu\int_{-\infty}^{\infty}\left[2Zn(x) - \frac{2\sigma}{e_0 D}\right]\mathrm{d}x\end{aligned} \tag{8}$$

In equilibrium,

$$\delta\int_{-\infty}^{\infty}\mathcal{F}\,\mathrm{d}x = 0 \tag{9}$$

Using expression (8) we can perform the first variation of F as follows:

$$\begin{aligned}\delta\mathcal{F} = \delta&\left(\frac{1}{8\pi l_B}\int_{-\infty}^{\infty}\Psi'^2\mathrm{d}x\right)\\ &+ \textstyle\int_{-\infty}^{\infty}\mathrm{d}x\;\delta n(x)[\ln(n(x)v_0) - \gamma\,\ln(1-n(x)v_0)]\\ &+ \textstyle\int_{-\infty}^{\infty}\mathrm{d}x\;\delta n(x)\langle p(s|x)[\ln p(s|x) + U(x)]\rangle\\ &+ \textstyle\int_{-\infty}^{\infty}\mathrm{d}x\;\delta n(x)\{\lambda(x)(\langle p(s|x)\rangle - 1) + 2Z\mu\}\\ &+ \textstyle\int_{-\infty}^{\infty}\mathrm{d}x\;\langle\delta p(s|x)n(x)[\ln p(s|x) + 1 + U(x) + \lambda(x)]\rangle\end{aligned} \tag{10}$$

We shall first perform the variation of the electrostatic energy (see the first term in Eq. (10)):

$$\delta\left(\frac{1}{8\pi l_B}\int_{-\infty}^{\infty}\Psi'^2\mathrm{d}x\right) = \frac{1}{4\pi l_B}\int_{-\infty}^{\infty}\Psi'\delta\Psi'\mathrm{d}x \tag{11}$$

Using per-partes integration the last term can be transformed into

$$\int_{-\infty}^{\infty} \Psi' \delta\Psi' \mathrm{d}x = \int_{-\infty}^{\infty} (\Psi \delta\Psi')' \mathrm{d}x - \int_{-\infty}^{\infty} \Psi \delta\Psi'' \mathrm{d}x \tag{12}$$

The first integral on the right side of Eq. (12) can be rewritten as

$$\int_{-\infty}^{\infty} (\Psi \delta\Psi')' \mathrm{d}x = \int_{-\infty}^{\infty} \mathrm{d}(\Psi \delta\Psi') = \Psi \delta\Psi'|_0^D \tag{13}$$

The surfaces at $x = 0$ and $x = D$ are uniformly charged, the variation of the first derivative of the potential at both charged surfaces is zero ($\delta\Psi'|_{x=0} = 0$ and $\delta\Psi'|_{x=D} = 0$) and the first integral on the right hand side of Eq. (12) is zero. Thus, Eq. (12) becomes

$$\int_{-\infty}^{\infty} \Psi' \delta\Psi' \mathrm{d}x = -\int_{-\infty}^{\infty} \Psi \delta\Psi'' \mathrm{d}x \tag{14}$$

We insert the Poisson equation

$$\Psi''(x) = -\varrho(x) \frac{4\pi l_B}{e_0} \tag{15}$$

into Eq. (12) and get

$$\delta\left(\frac{1}{8\pi l_B} \int_{-\infty}^{\infty} \Psi'^2 \mathrm{d}x\right) = \int_{-\infty}^{\infty} \Psi(x) \delta\left(\frac{\varrho(x)}{e_0}\right) \mathrm{d}x \tag{16}$$

where $\varrho(x)$ is the volume charge density.

Using the above derived relation (16) we can rewrite Eq. (10) as

$$\begin{aligned} \delta\mathcal{F} = & \int_{-\infty}^{\infty} \Psi(x) \delta\left(\frac{\varrho(x)}{e_0}\right) \mathrm{d}x \\ & + \int_{-\infty}^{\infty} \mathrm{d}x\ \delta n(x) [\ln(n(x)v_0) - \gamma \ln(1 - n(x)v_0)] \\ & + \int_{-\infty}^{\infty} \mathrm{d}x\ \delta n(x) \langle p(s|x) [\ln p(s|x) + U(x)] \rangle \\ & + \int_{-\infty}^{\infty} \mathrm{d}x\ \delta n(x) \{\lambda(x)(\langle p(s|x) \rangle - 1) + 2Z\mu\} \\ & + \int_{-\infty}^{\infty} \mathrm{d}x \langle \delta p(s|x) n(x) [\ln p(s|x) + 1 + U(x) + \lambda(x)] \rangle \end{aligned} \tag{17}$$

The volume charge density is determined by both charges of spheroidal nanoparticle:

$$\frac{\rho(x)}{Ze_0} = \langle n(x-s)p(s|x-s) + n(x+s)p(s|x+s)\rangle \tag{18}$$

The first variation of the volume charge density $\delta\varrho(x)$ is

$$\begin{aligned}\frac{\delta\rho(x)}{Ze_0} &= \langle \delta n(x-s)p(s|x-s) + n(x-s)\delta p(s|x-s)\rangle \\ &\quad + \langle \delta n(x+s)p(s|x+s) + n(x+s)\delta p(s|x+s)\rangle\end{aligned} \tag{19}$$

Inserting Eq. (19) into the first term of variation $\int_{-\infty}^{\infty}\Psi(x)\delta(\varrho(x)/e_0)\mathrm{d}x$ we get

$$\begin{aligned}&\int_{-\infty}^{\infty}\Psi(x)\delta\left(\frac{\varrho(x)}{e_0}\right)\mathrm{d}x \\ &= \int_{-\infty}^{\infty}\langle\Psi(x)Z[\delta n(x-s)p(s|x-s)+\delta n(x+s)p(s|x+s)]\rangle\mathrm{d}x \\ &\quad + \int_{-\infty}^{\infty}\langle\Psi(x)Z[n(x-s)\delta p(s|x-s)+n(x+s)\delta p(s|x+s)\mathrm{d}]\rangle x\end{aligned} \tag{20}$$

By introducing the new variables $\bar{x} = x + s$ and $\tilde{x} = x - s$, Eq. (20) can be rewritten as

$$\begin{aligned}&\int_{-\infty}^{\infty}\Psi(x)\delta\left(\frac{\varrho(x)}{e_0}\right)\mathrm{d}x \\ &= \int_{-\infty}^{\infty}\langle\delta n(x)p(s|x)[Z\Psi(x+s)+Z\Psi(x-s)]\rangle\mathrm{d}x \\ &\quad + \int_{-\infty}^{\infty}\langle n(x)\delta p(s|x)[Z\Psi(x+s)+Z\Psi(x-s)]\rangle\mathrm{d}x\end{aligned} \tag{21}$$

If we insert Eq. (21) into Eq. (17) we get

$$\begin{aligned}\delta F = &\int_{-\infty}^{\infty}\langle\delta n(x)p(s|x)[Z\Psi(x+s)+Z\Psi(x-s)]\rangle\mathrm{d}x \\ &+ \int_{-\infty}^{\infty}\langle n(x)\delta p(s|x)[Z\Psi(x+s)+Z\Psi(x-s)]\rangle\mathrm{d}x \\ &+ \int_{-\infty}^{\infty}\mathrm{d}x\delta n(x)[\ln n(x)\nu_0 - \gamma\ln(1-n(x)\nu_0)] \\ &+ \int_{-\infty}^{\infty}\mathrm{d}x\delta n(x)\langle p(s|x)[\ln p(s|x)+U(x)]\rangle \\ &+ \int_{-\infty}^{\infty}\mathrm{d}x\delta n(x)\{\lambda(x)(\langle p(s|x)\rangle - 1) + 2Z\mu\} \\ &+ \int_{-\infty}^{\infty}\mathrm{d}x\langle\delta p(s|x)n(x)[\ln p(s|x)+1+U(x)+\lambda(x)]\rangle\end{aligned} \tag{22}$$

Equation (9) has to be fulfilled for variations $\delta p(s|x)$ and $\delta n(x)$. This means that the expressions multiplied by $\delta p(s|x)$ and $\delta n(x)$ in Eq. (22) have to be zero. First, we consider the term multiplied by $\delta p(s|x)$:

$$\ln p(s|x) + 1 + U(x) + \lambda(x) + Z\Psi(x+s) + Z\Psi(x-s) = 0 \quad (23)$$

from which the conditional probability density can be calculated

$$p(s|x) = \exp[-Z\Psi(x+s) - Z\Psi(x-s) - 1 - U(x) - \lambda(x)] \quad (24)$$

The normalization condition (1) determines the local Lagrange parameter, and Eq. (24) becomes

$$p(s|x) = \frac{\mathrm{e}^{-Z\Psi(x+s)-Z\Psi(x-s)}}{\left\langle \mathrm{e}^{-Z\Psi(x+s)-Z\Psi(x-s)} \right\rangle} \quad (25)$$

We also consider the terms multiplied by $\delta n(x)$:

$$\begin{aligned} &\ln n(x)v_0 - \gamma \ln (1 - n(x)v_0) \\ &\quad + \langle p(s|x)[Z\Psi(x+s) + Z\Psi(x-s)] \rangle \\ &\quad + \langle p(s|x)[\ln p(s|x) + U(x)] \rangle + 2Z\mu = 0 \end{aligned} \quad (26)$$

2.1. Including the Excluded Volume Effect

In the following we consider the situation in which the excluded volume of the spheroidal nanoparticles is taken into account. Therefore, $\gamma = 1$.

By inserting Eq. (25) into Eq. (26) and setting $\gamma = 1$, we obtain the equation for the concentration:

$$n(x) = \frac{q(x)\mathrm{e}^{-U(x)-2Z\mu}}{v_0[1 + q(x)\mathrm{e}^{-U(x)-2Z\mu}]} \quad (27)$$

where we defined

$$q(x) = \left\langle \mathrm{e}^{-Z\Psi(x+s)-Z\Psi(x-s)} \right\rangle \quad (28)$$

The ionic distribution function can be obtained by inserting Eqs. (27) and (25) into equation $n(x,s) = n(x)p(s|x)$:

$$n(x,s) = \frac{\mathrm{e}^{-Z\Psi(x+s)-Z\Psi(x-s)-U(x)-2Z\mu}}{v_0[1 + q(x)\mathrm{e}^{-U(x)-2Z\mu}]} \quad (29)$$

The volume charge density (18) can then be rewritten in the form

$$\frac{\rho(x)}{Ze_0} = \langle n(x-s,s) + n(x+s,s)\rangle \tag{30}$$

where we took into account the definition of the ion distribution function.

By inserting Eq. (29) into Eq. (30) we get

$$\rho(x) = \frac{Ze_0}{\nu_0}\left\langle \frac{\mathrm{e}^{-Z\Psi(x)-Z\Psi(x-2s)-U(x-s)-2Z\mu}}{1+q(x-s)\mathrm{e}^{-U(x-s)-2Z\mu}} + \frac{\mathrm{e}^{-Z\Psi(x)-Z\Psi(x+2s)-U(x+s)-2Z\mu}}{1+q(x+s)\mathrm{e}^{-U(x+s)-2Z\mu}}\right\rangle \tag{31}$$

In the first term of Eq. (31) we replace $-s$ with s and add both terms

$$\rho(x) = \frac{2Ze_0}{\nu_0}\left\langle \frac{\mathrm{e}^{-Z\Psi(x)-Z\Psi(x+2s)-U(x+s)-2Z\mu}}{1+q(x+s)\mathrm{e}^{-U(x+s)-2Z\mu}}\right\rangle \tag{32}$$

By taking into account Eq. (28), Eq. (32) can be rewritten as

$$\rho(x) = \frac{2Ze_0}{\nu_0}\left\langle \frac{\mathrm{e}^{-Z\Psi(x)-Z\Psi(x+2s)-U(x+s)-2Z\mu}}{1+\left\langle \mathrm{e}^{-Z\Psi(x+\bar{s}+s)-Z\Psi(x-\bar{s}+s)}\right\rangle \mathrm{e}^{-U(x+s)-2Z\mu}}\right\rangle \tag{33}$$

The outer averaging is performed over s while the inner averaging is performed over $\bar{s}$.

Using the expression (33) for volume charge density $\varrho(x)$ in the Poisson Eq. (15) yields the integro-differential equation for the reduced electrostatic potential in the form

$$\Psi''(x) = -\frac{8\pi l_{\mathrm{B}} Z}{\nu_0}\left\langle \frac{\mathrm{e}^{-Z\Psi(x)-Z\Psi(x+2s)-U(x+s)-2Z\mu}}{1+\left\langle \mathrm{e}^{-Z\Psi(x+\bar{s}+s)-Z\Psi(x-\bar{s}+s)}\right\rangle \mathrm{e}^{-U(x+s)-2Z\mu}}\right\rangle \tag{34}$$

The boundary conditions for this integro-differential equation are given at the charged surfaces:

$$\Psi'(x=0) = -\frac{4\pi\sigma l_{\mathrm{B}}}{e_0}, \qquad \Psi'(x=D) = \frac{4\pi\sigma l_{\mathrm{B}}}{e_0} \tag{35}$$

2.2. Excluding the Excluded Volume Effect

Here we consider the situation in which the excluded volume effect of spheroidal nanoparticles is not taken into account. Therefore, $\gamma = 0$.

By inserting Eq. (25) into Eq. (26) and setting $\gamma = 0$, we obtain the equation for the concentration:

$$n(x) = \frac{q(x)}{\nu_0} \mathrm{e}^{-U(x) - 2Z\mu} \tag{36}$$

where $q(x)$ is given by Eq. (28). The ion distribution function can be obtained by inserting Eqs. (36) and (25) into equation $n(x,s) = n(x)p(s|x)$:

$$n(x,s) = \frac{1}{\nu_0} e^{-Z\Psi(x+s) - Z\Psi(x-s) - U(x) - 2Z\mu} \tag{37}$$

Again, the volume charge density (18) can then be rewritten in the form

$$\frac{\rho(x)}{Ze_0} = \langle n(x-s,s) + n(x+s,s) \rangle \tag{38}$$

where we took into account the definition of the ion distribution function.

Inserting Eq. (37) into Eq. (38) we get

$$\rho(x) = \frac{Ze_0}{\nu_0} \langle \mathrm{e}^{-Z\Psi(x) - Z\Psi(x-2s) - U(x-s) - 2Z\mu} + \mathrm{e}^{-Z\Psi(x) - Z\Psi(x+2s) - U(x+s) - 2Z\mu} \rangle \tag{39}$$

In the first term of Eq. (39) we replace $-s$ with s and add both terms:

$$\rho(x) = \frac{2Ze_0}{\nu_0} \langle \mathrm{e}^{-Z\Psi(x) - Z\Psi(x+2s) - U(x+s) - 2Z\mu} \rangle \tag{40}$$

The averaging is performed over s.

Using the expression (40) for volume charge density $\varrho(x)$ in Poisson Eq. (15) yields the integro-differential equation for the reduced electrostatic potential in the form

$$\Psi''(x) = -\frac{8\pi l_B Z}{\nu_0} \langle \mathrm{e}^{-Z\Psi(x) - Z\Psi(x+2s) - U(x+s) - 2Z\mu} \rangle \tag{41}$$

The boundary conditions for this integro-differential equation are given at the charged surfaces by Eq. (35).

2.3. Numerical Methods

The integro-differential Eq. (41) was solved numerically. The boundary value problem was restated as a fixed-point equation $\Psi = \mathcal{G}(\Psi)$, where $\mathcal{G}(\Psi)$ is the solution Ξ of the ordinary differential boundary value problem:

$$\Xi''(x) = -8\pi l_B \frac{1}{\nu_0} Z e^{-Z\Xi(x)-2Z\mu} \times \frac{1}{2l} \int_{\max[-l,\, l-x]}^{\min[l,\, D-x]} ds\, \exp(-Z\Psi(x+s)) \tag{42}$$

with boundary conditions

$$\Xi'(x=0) = -\frac{\sigma e}{\varepsilon k T} \tag{43}$$

$$\Xi'(x=D) = \frac{\sigma e}{\varepsilon k T} \tag{44}$$

The domain $[0, D]$ was represented by a mesh of N Chebyshev nodes, the function Ψ by an N-dimensional vector Ψ_N of values of Ψ at the mesh nodes, and the fixed-point equation was discretized into a finite dimensional algebraic equation $\Psi_N = \pi_N\left[\mathcal{G}\left(_{pN}(\Psi_N)\right)\right]$, where $p_N(\Psi_N)$ is the interpolating polynom through the values of Ψ_N at the mesh nodes and $\pi_N(\Xi)$ is the N-dimensional vector representing the values of the function Ξ at the mesh nodes. The discretized fixed-point equation was rewritten as $G[\Psi_N] = \Psi_N - \pi_N\left[\mathcal{G}\left(_{pN}(\Psi_N)\right)\right] = 0$ and then solved by "fsolve" MATLAB function (available in the optimization toolbox), which finds solutions of nonlinear algebraic equations by a least-squares method. The function "fsolve" requires the solution of the above-defined second-order ordinary boundary value problem which was restated as a system of first-order equations and solved by the "bvp4c" MATLAB function by collocation. The integral in the second-order ordinary boundary value problem was computed by the "quad" MATLAB function.

2.4. Monte Carlo Simulation

In the simulation, the standard Monte Carlo Metropolis algorithm [60] with Lekner periodic boundary conditions [61] in the directions parallel to the charged walls was used. A system of 100–200 spheres confined between two

impenetrable charged surfaces was considered. Translational and rotational moves were taken into account. To make contact with the theory, the hard core interaction between particles and the walls was taken into account by means of the distance of the closest approach. The influence of the direct hard core interaction between spheres on the charge density distribution was also calculated for two cases (Figs. 4 and 5).

3. Results

Electrostatic potential Ψ, volume charge density ρ, orientational order parameter S, and free energy F of the system are calculated for different values of model parameters: surface charge density σ, size of the spherical particles which corresponds to the distance between both charges l and distance between the charged surfaces D. The minimal distance D we can achieve is equal to the size of the particles l [when density of the particles (surface charge density) is not too high]. We keep constant valency of the charges $Z = 1$, which are positioned on the surface of the sphere ($l = a$).

Electrostatic potential between the charged surfaces is obtained for three different particle sizes at a distance between the surfaces $D = 20$ nm, which is much larger than the diameter of the particles l (Fig. 3A). We observe that the electrostatic potential monotonously decreases with increasing distance from the left charged surfaces and reaches its minimal value in the midplane. The slope of the electrostatic potential changes essentially at the distance

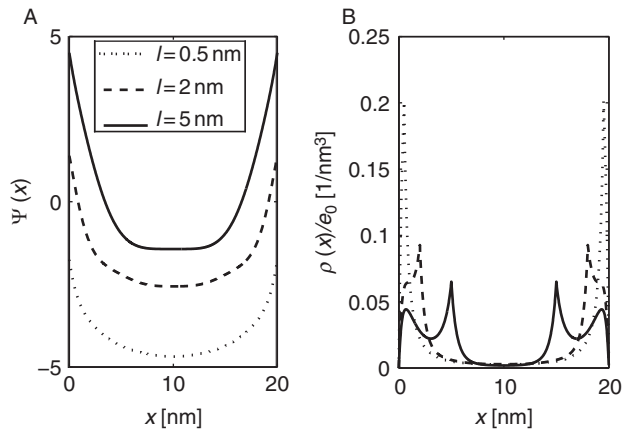

Figure 3 (A) Electrostatic potential Ψ and (B) volume charge density ρ as functions of the distance from the left charged surface x for three different diameters of the spheroidal nanoparticles. The model parameter is $|\sigma| = 0.033$ As/m^2.

$x \cong l$ from the charged surface for all values of l. In Fig. 3B we present the volume charge density distribution between both surfaces.

We can see one peak in the volume charge density near each surface for small particles ($l = 0.5$ nm). If we increase l, an additional minimum appears at $x \approx l/2$ (see full line in Fig. 3B). The reason for the existence of the additional minimum is that the probability to find nanoparticles with the center at $x = l/2$ which are oriented parallel to the surfaces decreases with increasing dimension of the nanoparticles.

It can be seen in Fig. 3 that for small particles in the limit of vanishing l, the electrostatic potential $\psi(x)$ as well as charge density distribution $\rho(x)$ converge towards the corresponding potential and concentration obtained by standard PB theory for point-like particles.

Although in the theory direct particle–particle interactions are not explicitly taken into account (since the theory is essentially the mean field approach), comparison of calculated volume charge density distribution with corresponding Monte Carlo simulations shows satisfactory agreement (Figs. 4 and 5). By using Monte Carlo simulations, we also checked the influence of the particle–particle hard core interactions which are not taken into account in the theoretical model. It can be seen in Fig. 4 that for distance $D = 2.5$ nm there is practically no difference in volume charge density profile between the predictions of theoretical model and Monte Carlo simulations. This ceases to be true when the distance between the surfaces is increased to $D = 4$ nm at the same surface charge density $|\sigma| = 0.033$ As/m^2 and the same size of the particles $l = 2$ nm (Fig. 5). Taking into account the particle–particle hard core interactions in MC

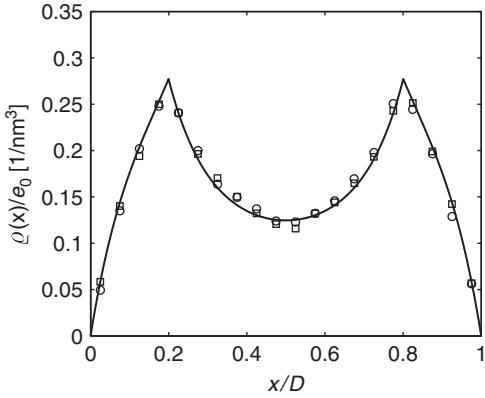

Figure 4 Influence of the hard core interaction between the spherical particles on the volume charge density $\rho(x)$ calculated for surface charge density $|\sigma| = 0.033$ As/m^2 and distance between the charged surfaces: $D = 2.5$ nm (squares: MC simulation with hard core interaction; circles: MC simulation without hard core interaction; solid line: theoretical prediction).

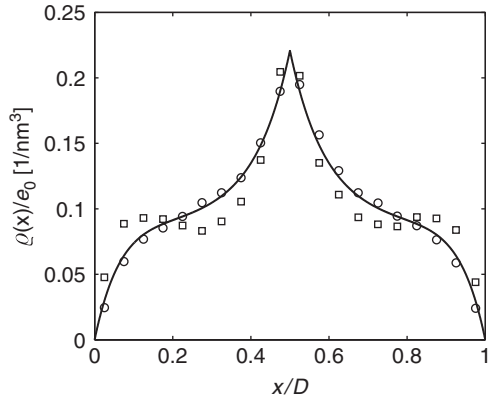

Figure 5 Influence of the hard core interaction between the spherical particles on the volume charge density $\rho(x)$ calculated for surface charge density $|\sigma| = 0.033$ As/m^2 and distance between the charged surfaces: $D = 4$ nm (squares: MC simulation with hard core interaction; circles: MC simulation without hard core interaction; solid line: theoretical prediction).

simulations, two peaks in $\rho(x)$ appear for $D = 4$ nm (Fig. 5), which means that the orientation of the particles is slightly stronger if the hard core interactions are taken into account. Therefore, the effects predicted by the theory are expected to be even more expressed because of the hard core interactions.

Figure 6 shows the average order parameter $S = \langle(3cos^2\vartheta - 1)/2\rangle$ as a function of the distance between the charged surfaces D. The angle ϑ describes the angle between the line connecting both charges of the nanoparticle (Fig. 1) and the x-axis. The dependence of S on the distance D exhibits a maximum at D slightly larger than the size of the particles l, then it falls down with increasing D to nearly fixed value and practically remains the same for any larger distance D. Monte Carlo results agree well with theoretical predictions, especially at smaller distances. For larger values of the surface charge density σ, the dependency $S(D)$ is shifted up, while it is decreased for smaller values of σ [26]. Figure 7 shows the order parameter S in dependence on the distance of the center of the spherical nanoparticles from the charged surface (x_c) for different values of surface charge density σ and the distance between the surfaces $D = 2.5$ nm. The order parameter S increases with increasing surface charge density $|\sigma|$ and exhibits two maxima near the charged surfaces (especially for higher surface charge densities), which means that the ordering near the charged surfaces is stronger than far from the surfaces.

The orientational ordering effect which we already observed in the volume charge density distribution and in the spatial dependency of the order parameter is also reflected in the free energy calculations. We consider

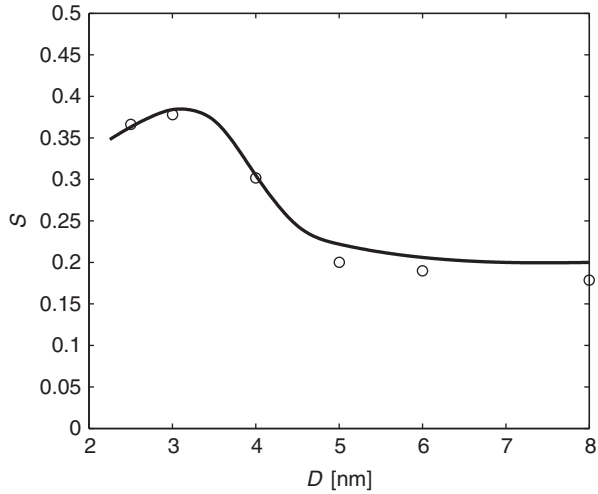

Figure 6 The average order parameter $S = \langle(3cos^2\vartheta - 1)/2\rangle$, where ϑ is the angle between the main axis of nanoparticles and the x-axis. In dependence on the distance between the charged surfaces D for $l = 2$ nm, $|\sigma| = 0.07$ As/m^2.

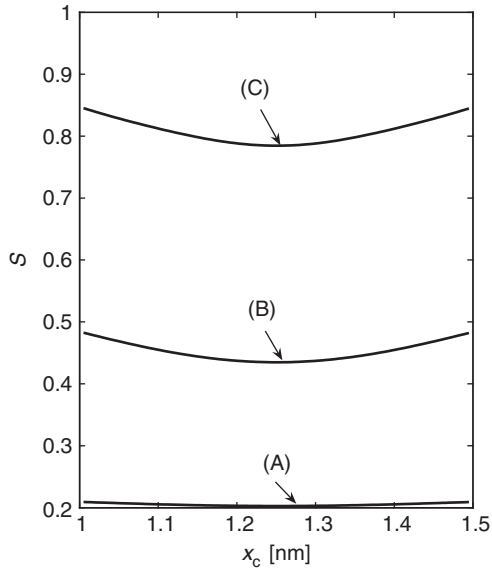

Figure 7 The order parameter S of spherical counterions as a function of the average position of their centers x_c for the distance between the charged walls $D = 2.5$ nm and diameter of ions 2 nm. The surface charge densities are (A) $|\sigma| = 0.033$ As/m^2, (B) $|\sigma| = 0.1$ As/m^2, and (C) $|\sigma| = 0.4$ As/m^2.

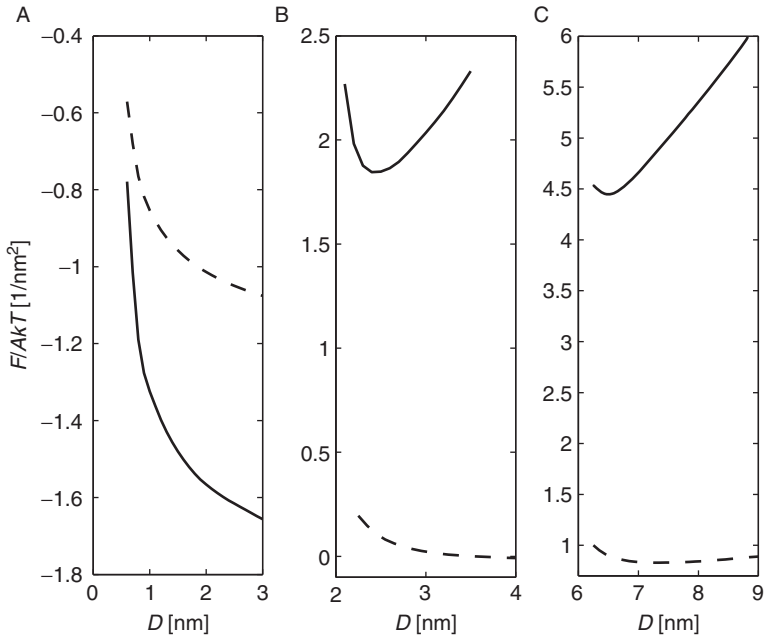

Figure 8 Electrostatic free energy F, measured per unit area of the charged surface A and per thermal energy kT as a function of the distance between two equally charged plates D for two different surface charge densities (solid lines: $|\sigma| = 0.1$ As/m^2, dashed lines: $|\sigma| = 0.033$ As/m^2). The diameters of the spheres are (A) $l = 0.5$ nm, (B) and $l = 2$ nm, and (C) $l = 6$ nm.

the interaction between two like-charged planar surfaces as a function of the distance D between them. The electrostatic free energy as a function of D is shown in Fig. 8 for two surface charge densities and for three sizes of the particles: $l = 6$ nm, $l = 2$ nm and $l = 0.5$ nm. It can be seen in Fig. 8A and B that for small surface charge density $|\sigma| = 0.033$ As/m^2, for the size of the particles $l = 0.5$ nm and $l = 2$ nm, the interaction between charged surfaces is repulsive, meanwhile for very large particles ($l = 6$ nm), the interaction also becomes attractive for small surface charge density σ with the minimum of the free energy at the value of D slightly larger than the size of the particles. On the other hand, the interaction between the like-charged surfaces is attractive for large surface charge densities (e.g., $|\sigma| = 0.1$ As/m^2) and large enough diameter of the nanoparticle ($l = 6$ nm or $l = 2$ nm). In this case the repulsive behavior is observed only when the size of particles decreases below a certain value and approaches to the limit of point particles (see Fig. 8A). When the attraction between like-charged surfaces is predicted, the minima in the free energy occur at distances D close to the size of the particles l. Based on presented results it can be therefore

concluded that the particle size plays a decisive role in the free energy dependency on the distance D and can revert the system from repulsive to attractive regime. As we have shown before, the orientational order parameter of the particles increases with decreasing distance between the surfaces D and with increasing surface charge density $|\sigma|$, indicating that orientational ordering of the particles near the surfaces mediates attractive interaction between the two like-charged surfaces.

4. Concluding Remarks

We studied the interactions between equally charged planar surfaces in a solution containing large multivalent spheroidal nanoparticles, that is, counterions with two charges placed diametrically on the surface of the nanoparticle. The distance of closest approach of the center of spherical nanoparticles to the charged surfaces was taken into account as the boundary condition for distribution of nanoparticles. Particle–particle hard core interactions were not taken into account in presented theoretical predictions, which according to our opinion leads to underestimation of the predicted attractive force. Although ion–ion interactions are not taken into account within the mean field approach, the comparison of the predicted volume charge density distribution with the corresponding results of the Monte Carlo simulations shows a good agreement, meaning that direct interactions do not play a major role in this case. The internal charge distribution with spatially separated charges within a single nanoparticle is reflected in intraionic correlations. Within the presented theoretical model, the expression for the free energy of the system contains in addition to usual electrostatic and entropic contribution to the free energy also the term due to orientational ordering of nanoparticles which is in our system the main reason for the predicted attractive interaction between the like-charged surfaces [27].

For large enough diameters of the multivalent spheroidal nanoparticles, the attraction between the equally charged surfaces takes place even at small surface charge densities. Attraction occurs at smaller sizes of the particles if the surface charge density of charged surfaces is large enough, which means that either the surface charge density or the size of the particles has to be large to yield attraction between like-charged surfaces. In the limit of the point-like particles, the presented theory reduces to PB theory where attraction between equally charged surfaces cannot be obtained.

The fact that the distance between the charged surfaces with minimal free energy is close to the diameter of the nanoparticles (Fig. 8), indicates that the bridging mechanism plays an important role in the predicted attractive force between like-charged surfaces [49, 62]. The calculated orientational order parameter (Fig. 6) shows that the most probable

orientation of spheroidal nanoparticles coincides with the orientation of the particle's main axis (connecting the two charges) in perpendicular direction to the charged planar surfaces. The two point charges of the nanoparticle (Fig. 1) energetically prefer to be in close vicinity of both charged surfaces, so they connect them as a bridge which is most efficient when the distance between the charged surfaces becomes comparable to the distance between the two charges of the nanoparticle.

Our results could be used to explain the behavior of more complicated systems such as large spherical membrane surfaces immersed in a solution composed of complex nanoparticles with spatially distributed charges.

In biological systems, a relevant system is composed of negatively charged membranes in the solution containing large multivalent ions, such as in blood where blood cells and derived membranous vesicular structures are immersed in plasma. According to our results, proteins with dimeric distribution of localized positive charge (such as some antibodies) can mediate attractive interaction between negatively charged membranous structures. Indeed, it has been observed that anticardiolipin antibodies induce the coalescence of negatively charged phospholipid vesicles.

Mediated interaction between like-charged membranes may have an important impact on the process of microvesiculation of the cell membrane. Microvesicles are formed in the final stage of the process of membrane budding, that is, when the bud is pinched off the mother membrane to become a free microvesicle. While narrowing of the neck connecting the bud and the mother membrane, the membranes of the bud and of the mother membrane are in close proximity and are subject to the short-ranged interaction mediated by the plasma proteins. Proteins with appropriate distribution of charge act as mediators of the attractive interaction and cause adhesion of the bud to the mother membrane, thereby preventing the bud to become free microvesicle. Since microvesicles are prothrombogenic, the mediating effect of certain plasma proteins can be interpreted as an anticoagulant effect of plasma proteins. The results presented in this work may therefore add to a better understanding of the mechanisms that are important for the formation of blood clots.

REFERENCES

[1] S. McLaughlin, The electrostatic properties of membranes, Annu. Rev. Biophys. Biophys. Chem. 18 (1989) 113–136.
[2] G. Cevc, Membrane electrostatics, Biochim. Biophys. Acta 1031 (1990) 311–382.
[3] A. Iglič, M. Brumen, S. Svetina, Determination of the inner surface potential of the erythrocyte membrane, Bioelectrochem. Bioenerg. 43 (1997) 97–103.
[4] H. Hägerstrand, B. Isomaa, Lipid and protein composition of exovesicles released from human erythrocytes following treatment with amphiphiles, Biochim. Biophys. Acta 1190 (1994) 409–415.

[5] H. Hägerstrand, V. Kralj-Iglič, M. Bobrowska-Hägerstrand, A. Iglič, Membrane skeleton detachment in spherical and cylindrical microexovesicles, Bull. Math. Biol. 61 (1999) 1019–1030.
[6] M. Sorice, A. Circella, R. Misasi, V. Pittoni, T. Garofalo, A. Cirelli, A. Pavan, G.M. Pontieri, G. Valesini, Cardiolipin on the surface of apoptotic cells as a possible trigger for antiphospholipid antibodies, Clin. Exp. Immunol. 122 (2000) 277–284.
[7] M.C. Martinez, A. Tesse, F. Zobairi, R. Andriantsitohaina, Shed membrane microparticles from circulating and vascular cells in regulating vascular function, Am. J. Physiol. Heart Circ. Physiol. 288 (2005) H1004–H1009.
[8] T.J. Greenwalt, The how and why of exocytic vesicles, Transfusion 46 (2006) 143–152.
[9] K. Balasubramanian, J. Chandra, A.J. Schroit, Immune clearance of phosphatidylserine-expressingcells by phagocytes, J. Biol. Chem. 272 (1997) 31113–31117.
[10] S.K. Moestrup, I. Schousboe, C. Jacobsen, J.R. Leheste, E.I. Christensen, T.E. Willnow, Beta2-glycoprotein-I (apolipoprotein H) and beta2-glycoprotein-I-phospholipid complex harbor a recognition site for the endocytic receptor megalin, J. Clin. Invest. 102 (1998) 902–909.
[11] P. Thiagarajan, A. Le, C.R. Benedict, β2-Glycoprotein I promotes the binding of anionic phospholipid vesicles by macrophages, Arterioscler. Thromb. Vasc. Biol. 19 (1999) 2807–2811.
[12] B. Bouma, P.G. de Groot, J.M.H. van den Elsen, R.B.G. Ravelli, A. Schouten, M.J.A. Simmelink, Adhesion mechanism of human β_2-glycoprotein I to phospholipids based on its crystal structure, EMBO J. 18 (1999) 5166–5174.
[13] J. Marra, Direct measurement of the interaction between phosphatidylglycerol bilayers in aqueous electrolyte solutions, Biophys. J. 50 (1986) 815–825.
[14] R. Kjelander, S. Marčelja, R.M. Pashley, J.P. Quirk, Double-layer ion correlation forces restrict calcium-clay swelling, J. Phys. Chem. 92 (1988) 6489–6492.
[15] M. Dubois, T. Zemb, N. Fuller, R.P. Rand, V.A. Parsegian, Equation of state of a charged bilayer system: Measure of the entropy of the lamellar–lamellar transition in DDABr, J. Chem. Phys. 108 (1998) 7855–7869.
[16] V.A. Bloomfield, DNA condensation, Curr. Opin. Struct. Biol. 6 (1996) 334–341.
[17] V. Teif, Ligand-induced DNA condensation: Choosing the model, Biophys. J. 89 (2005) 2574–2587.
[18] I. Rouzina, V. Bloomfield, Macroion attraction due to electrostatic correlation between screening counterions. 1. Mobile surface-adsorbed ions and diffuse ion cloud, J. Phys. Chem. 100 (1996) 9977–9989.
[19] T.E. Angelini, H. Liang, W. Wriggers, G.C.L. Wong, Like-charge attraction between polyelectrolytes induced by counterion charge density waves, Proc. Natl. Acad. Sci. USA 100 (2003) 8634–8637.
[20] W.M. Gelbart, R. Bruinsma, P.A. Pincus, V.A. Parsegian, DNA-inspired electrostatics, Phys. Today 53 (2000) 38–44.
[21] J.C. Butler, T. Angelini, J.X. Tang, G.C.L. Wong, Ion multivalence and like-charge polyelectrolyte attraction, Phys. Rev. Lett. 91 (2003) 028301.
[22] D.F.H. Evans Wennerström, The Colloidal Domain: Where Physics, Chemistry, Biology, and Technology Meet. (1994) VCH Publishers, New York.
[23] J.N. Israelachvili, Intermolecular and Surface Forces. (1997) Academic Press, London.
[24] E. Verwey, J. Overbeek, Theory of the Stability of Lyophobic Colloids. (1948) Elsevier Publishing Company Inc.
[25] J. Sadar, D. Chan, Long-range electrostatic attractions between identically charged particles in confined geometries and the Poisson–Boltzmann theory, Langmuir 16 (2000) 324–331.
[26] J. Urbanija, K. Bohinc, A. Bellen, S. Maset, A. Iglič, V. Kralj-Iglič, P.B. Sunil Kumar, Attraction between negatively charged surfaces mediated by spherical counterions with quadrupolar charge distribution, J. Chem. Phys. 129 (2008) 105101.

[27] K. Bohinc, A. Iglič, S. May, Interaction between macroions mediated by divalent rodlike ions, Europhys. Lett. 68 (2004) 494–500.
[28] A.G. Moreira, R. Netz, Simulations of counterions at charged plates, Eur. Phys. J. E 8 (2002) 33–58.
[29] L. Guldbrand, B. Jönsson, H. Wennerström, P. Linse, Electrical double layer forces. A Monte Carlo study, J. Chem. Phys. 80 (1984) 2221–2228.
[30] B. Svensson, B. Jönsson, Chem. Phys. Lett. 108 (1984) 580.
[31] D. Bratko, V. Vlachy, Distribution of counterions in the double layer around a cylindrical polyion, Chem. Phys. Lett. 90 (1982) 434–438.
[32] R. Kjellander, S. Marčelja, Chem. Phys. Lett. 112 (1984) 49.
[33] H. Greberg, R. Kjellander, Charge inversion in electric double layers and effects of different sizes for counterions and coions, J. Chem. Phys. 108 (1998) 2940–2953.
[34] R. Kjellander, Ion–ion correlations and effective charges in electrolyte and macroion systems, Berichte der Bunsen-Gesellschaft 100(6) (1996) 894–904.
[35] V. Vlachy, Ionic effects beyond Poisson–Boltzmann theory, Annu. Rev. Phys. Chem. 50 (1999) 145–165.
[36] M. Stevens, M. Robbins, Density functional theory of ionic screening: When do like charges attract? Europhys. Lett. 12 (1990) 81.
[37] Z. Tang, L. Scriven, H. Davis, Interactions between primitive electrical double layers, J. Chem. Phys. 97 (1992) 9258–9266.
[38] A. Diehl, M. Tamashiro, M. Barbosa, Y. Levin, Density-functional theory for attraction between like-charged plates, Physica A 274 (1999) 433.
[39] J. Forsman, A simple correlation-corrected Poisson–Boltzmann theory, J. Phys. Chem. B 108(26) (2004) 9236–9245.
[40] P.A. Pincus, S.A. Safran, Charge fluctuations and membrane attractions, Europhys. Lett. 42 (1998) 103–108.
[41] D.B. Lukatsky, S.A. Safran, Pressure of correlated layer-charge and counterion fluctuations in charged thin films, Phys. Rev. E 60 (1999) 5848–5857.
[42] A.W.C. Lau, D.B. Lukatsky, P. Pincus, S.A. Safran, Charge fluctuations and counterion condensation, Phys. Rev. E 65 (2002) 051502.
[43] T. Akesson, C. Woodward, B. Jonsson, Electric double layer forces in the presence of polyelectrolytes, J. Chem. Phys. 91 (1989) 2461–2469.
[44] I. Borukhov, D. Andelman, H. Orland, Effect of polyelectrolyte adsorption on intercolloidal forces, J. Phys. Chem. B 103 (1999) 5042–5057.
[45] A. Watts (Ed.), Protein–Lipid Interactions (1993) Elsevier.
[46] N. Ben-Tal, B. Honig, C. Miller, S. McLaughlin, Electrostatic binding of proteins to membranes. Theoretical predictons and experimental results with charybdotoxin and phospholipid vesicles, Biophys. J. 73 (1997) 1717–1727.
[47] D. Murray, A. Arbuzova, G. Hangyas-Mihalyne, A. Gambhir, N. Ben-Tal, B. Honig, S. McLaughlin, Electrostatic properties of membranes containing acidic lipids and adsorbed basic peptides: Theory and experiment, Biophy. J. 77 (1999) 3176–3188.
[48] D. Murray, S. McLaughlin, B. Honig, The role of electrostatic interactions in the regulation of the membrane association of G protein $\beta\gamma$ heterodimers, J. Biol. Chem. 276 (2001) 45153–45159.
[49] R. Podgornik, Polyelectrolyte-mediated bridging interactions, J. Polym. Sci.: Part B: Polym. Phys. 42 (2004) 3539–3556.
[50] B. Yoon, A. Lenhoff, Computation of the electrostatic interaction energy between a protein and a charged surface, J. Phys. Chem. 96 (1992) 3130–3134.
[51] V. Kralj-Iglič, A. Iglič, A simple statistical mechanical approach to the free energy of the electric double layer including the excluded volume effect, J. Phys. II (France) 6 (1996) 477–491.

[52] E. Trizac, J. Raimbault, Long-range electrostatic interactions between like-charged colloids: steric and confinement effects, Phys. Rev. E 60 (1999) 6530–6533.
[53] P.M. Biesheuvel, M. van Soestbergen, Counterion volume effects in mixed electrical double layers, J. Colloid Interface Sci. 316(2) (2007) 490–499.
[54] M.V. Fedorov, A.A. Kornyshev, Ionic liquid near a charged wall: Structure and capacitance of electrical double layer, J. Phys. Chem. B 112(38) (2008) 11868–11872.
[55] W. Fawcett, Charge distribution effects in the solution chemistry of polyatomic ions, Condens. Matter Phys. 8 (2005) 413–424.
[56] A. Razinger, A. Iglič, V. Kralj-Iglič, Orientation of multivalent ions near charged planar surfaces, J. Phys. A: Math. Gen. 39 (2006) 3275–3282.
[57] N. Cuvillier, F. Rondelez, Breakdown of the Poisson–Boltzmann description for electrical double layers involving large multivalent ions, Thin Solid Films 327–329 (1998) 19–23.
[58] J.C. Jackson, Classical Electrodynamics. (1999) John Wiley and Sons. Inc., New York.
[59] K. Bohinc, V. Kralj-Iglič, A. Iglič, Thickness of electrical double layer. Effect of ion size, Electrochim. Acta 46 (2001) 3033–3040.
[60] D. Frenkel, B. Smit, Understanding Molecular Simulations Academic. (1996) New York.
[61] J. Lekner, Summation of coulomb fields in computer-simulated disordered systems, Physica A 176 (1991) 485.
[62] A.Yu. Grosberg, T.T. Nguyen, B.I. Shklovskii, Colloquium: The physics of charge inversion in chemical and biological systems, Rev. Mod. Phys. 74 (2002) 329.